

SIMULATION OF SPEED CONTROL OF SWITCHED RELUCTANCE MOTOR USING ANFIS

¹V. RAVI TEJA, ²RAJU LAKSHMANA REDDY

¹M-tech student Scholar, Department of Electrical & Electronics Engineering, Velaga Nageswara Rao College of Engineering, Ponnuru; Guntur (Dt); A.P, India.

²M-Tech, Associate Professor, Department of Electrical & Electronics Engineering, Velaga Nageswara Rao College Of Engineering, Ponnuru; Guntur (Dt); A.P,

Abstract —This paper develops an ANFIS based torque control of SRM to reduce the torque ripple. The ANFIS has the advantages of expert knowledge of the fuzzy inference system and the learning capability of neural networks. This controller realizes a good dynamic behavior of the motor, a perfect speed tracking with no overshoot and a good rejection of impact loads disturbance. The results of applying the adaptive neuro-fuzzy controller to a SRM give better performance and high robustness than those obtained by the application of a conventional controller (PI). The above controller was realized using MATLAB/Simulink.

Index Terms— ANFIS, Torque Control, Switched Reluctance Motor.

I. INTRODUCTION

With concerns over energy efficient drive, Switched Reluctance Motor (SRM) has attracted the interest in fields of Electric Vehicle (EV) due to its robust construction, fault tolerant operation, high starting torque without the problem of excessive inrush current, and high-speed operation. However, SRM suffers from some drawbacks such as high torque ripple and acoustic noise which are very critical for EV applications. The research is progressing extensively for the mitigation of torque ripple and acoustic noise. In indirect torque control scheme of SRM, the torque of the motor is controlled by controlling the motor current. Due to high nonlinearity in torque and current relationship, the conversion of torque into equivalent current value is cumbersome. In the paper [1], the torque is directly proportional to the ideal phase inductance profile which increases or decreases proportionately with the angle of overlap.

Due to magnetic saturation, the phase inductance varies with the motor current which leads to large amount of error in both instantaneous and average value of torque. In [2], the author had suggested a multiplication factor F to compensate for the error of torque and F should be a function of current level. In [3], the author have suggested approximating the torque as proportional to the square of stator current, where the multiplying factor is assumed to vary as a sinusoidal function of rotor position alone. A two dimensional lookup table in which the torque value is stored as function of current and rotor position. The amount of time taken for computation of torque is very high [4, 5]. In [6], a Cerebellar Model Articulation Controller (CMAC) based torque control was presented. A closed loop torque controller based on B-spline neural network (BSNN) with online training was presented in [7]. Back-propagation (BP) based neural network controllers have been proposed in

[8]-[10], but both of [8] and [9] used one-hidden-layer neural network which is not sufficient for estimating the stabilized motor current. In [11, 12], look-up tables were generated off-line by building an SRM model to profile the current for the flat torque waveform and stored in the controller. During on-line running, the controller searched the look-up tables for the current command.

Another comprehensive controller to maximize efficiency and peak overload capability of SRM by using look-up tables for electric vehicle drives has been designed. This controller has several look-up tables for different voltages. To calculate the control parameters for a certain torque - command/rotor-speed (operating point) and bus voltage, three interpolations have to be performed. The percentage error depends upon the resolution of lookup tables. At low speed, the torque ripple is sensitive to the current profile, and a slight deviation from the required profile may produce high torque ripple. In this paper, ANFIS based Direct Control of torque is proposed to minimize the torque ripple at low speed for its simple, easy to implement and fast dynamics. Computed results show that the proposed scheme can reduce the torque ripple and provide good dynamic performance with respect to changes in the torque commands.

Fig.1 shows a typical control diagram for SRM driven by asymmetric half bridges. Current controller is employed to generate switching signals for the asymmetric half bridges according to the current reference. The current reference is either given by a speed controller or a torque

distributor. If the current reference comes directly from a speed controller, flat top chopping current for each phase is employed. Due to the strong nonlinearity, in some cases, the flat top chopping current regulation might not provide satisfactory performance. Therefore, torque sharing control is used to distribute torque production between two phases in order to produce constant torque [2]-[7].

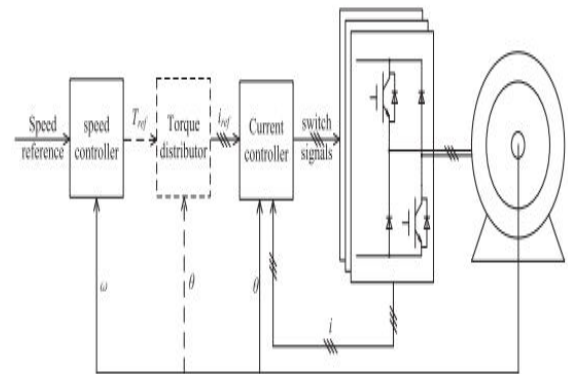


Fig..1. Typical SRM control diagram

Both flat top chopping current regulation and torque sharing control rely on accurate current controllers. Hysteresis control is one of the most popular current control schemes in SRMs, due to its fast dynamic response and model independency [4]-[8]. However, hysteresis controller also suffers from drawbacks including variable switching frequency and very high sampling rate [9]-[11]. Variable switching frequency in hysteresis control makes it difficult to design the electromagnetic interference(EMI) filter and may cause an acoustical noise. High-speed ADCs have higher sampling rate, however, they add additional cost to the SRM drive system.

In order to avoid the drawbacks of the hysteresis current controller, fixed frequency PWM controllers have been



studied[9], [11]–[16]. In [12], an open loop PWM controller is used, whereas in [9], a proportional-integral (PI) current controller has been investigated and a current sampling method for digital control have been introduced. A proportional (P) controller with an iterative learning control is proposed in [17] to achieve accurate current control. In [11], [13]–[16], back EMF compensation to the PI current controller has been analyzed. In [11], the gains of the PI controller are adjusted according to current and rotor position. However, a PI controller suffers from either slow response or possible overshoot. It is also difficult to tune the PI controller in SRM applications due to the highly nonlinear characteristics of the machine.

Model-based dead-beat flux controller are proposed in [18]–[21]. The dead-beat controller achieves constant switching frequency and lower sampling rate, while maintaining the similar dynamic response as hysteresis controller. However, the performance of a dead-beat controller relies on an accurate model and a large gain, which may degrade the performance of the dead-beat controller.

In [22], a Lyapunov function-based controller is proposed to solve model mismatch issue. The tracking error is bounded by the parameters of the controller. A sliding mode current controller is proposed in [23]. Parameters of these controllers are carefully selected according to the model mismatch. These control methods need to store several look-up tables, which increase the storage and computational burden of the digital controller.

A digital PWM current controller for the SRM drives is proposed in this paper in order to achieve fast response, accurate tracking, immunity to noise, model mismatch, and stability. The proposed controller takes full advantage of the model information. Smaller feedback gain could be chosen in order to reduce noise sensibility without degrading the performance. Parameter adaption is adopted to deal with the model mismatch. Relationships between the proposed controller and the previous mentioned PI dead-beat controllers are discussed. Both the simulation and experimental results are provided to verify the performance of the proposed current controller.

(II) MODEL OF SRM

By neglecting mutual coupling between phases, the phase voltage equation of an SRM can be given as

$$u_w = R_w \cdot i + \frac{d\psi(\theta, i)}{dt} \quad (1)$$

Where u_w is the phase voltage applied on the phase winding, R_w is the winding resistance, ψ is the flux linkage, θ is the rotor position, and i is the phase current.

Due to its double salient structure and saturation, ψ is a nonlinear function of both i and θ . Fig. 2 shows the measured flux linkage profile of the SRM studied in this paper. The rotor spins 360° per electric period. The aligned positions are 0° and 360° . The unaligned position is 180° . Fig. 2 could be stored into a lookup table when digital control is applied.

Considering the modeling errors, the real flux linkage is represented as



$$\psi(\theta, i) = \alpha \psi_m(\theta, i) \quad (2)$$

where ψ is the modeled flux linkage profile used in the controller, and factor α is a positive number that donates the relationship between the modeled flux linkage profile and the real one.

In the ideal case, the modeled flux linkage profile exactly matches the real one, and $\alpha = 1$. But in practice, no matter whether ψ_m is obtained by the experimental measurement or by an FEA calculation, there may be some mismatch between ψ and ψ_m . In this case, ψ_m is unknown and α may be variable and there is

$$\begin{aligned} \alpha &> 0 \\ \bar{\alpha} - B_{\alpha} &\leq \alpha \leq \bar{\alpha} + B_{\alpha} \\ |\dot{\alpha}| &\leq B_{\dot{\alpha}} \end{aligned} \quad (3)$$

where $\bar{\alpha}$ is the average value of α , $B_{\alpha} \geq 0$ is the variation bound of α , and $B_{\dot{\alpha}} \geq 0$ is the maximum variation rate of α . The values of B_{α} and $B_{\dot{\alpha}}$ depend on the modeling errors of the studied motor.

Considering the resistances and voltage drops on windings and switches, the phase voltage equation could be written as

$$\begin{aligned} \frac{d\psi_m(\theta, i)}{dt} &= -\frac{1}{\alpha} (R_w + R_c) i \\ &\quad - \frac{1}{\alpha} \left(\psi_m(\theta, i) \frac{d\alpha}{dt} + v_c + v_m + v_n \right) + \frac{1}{\alpha} u_c \end{aligned} \quad (4)$$

where u_c donates the converter output voltage, R_c donates the equivalent resistance of the converter, R_c could be obtained from either experiments or data sheets, but it changes according to current, temperature, gate source (GS) voltage, etc. v_c donates the voltage drop on the converter, v_m donates the voltage drop caused by mutual inductance, v_n reflects all other voltage

drops, and noises in the system. Equation (4) could be formulated as

$$\begin{aligned} \frac{d\psi_m(\theta, i)}{dt} &= -\frac{1}{\alpha} R i - \frac{1}{\alpha} v + \frac{1}{\alpha} u_c \\ R &= R_w + R_c \\ v &= \psi_m(\theta, i) \frac{d\alpha}{dt} + v_c + v_m + v_n \end{aligned} \quad (5)$$

where R is the total equivalent resistance and v is the total equivalent voltage drop. They are uncertain parameters that are not easy to model. The values of R and v are both unknown and may be variable, which are represented as

$$\begin{aligned} R &> 0 \\ \bar{R} - B_R &\leq R \leq \bar{R} + B_R \\ |\dot{R}| &\leq B_{\dot{R}} \\ \bar{v} - B_v &\leq v \leq \bar{v} + B_v \\ |\dot{v}| &\leq B_{\dot{v}} \end{aligned} \quad (6)$$

where \bar{R} donates the average value of R , $B_R \geq 0$ donates the variation bound of R , and $B_{\dot{R}} \geq 0$ donates the maximum variation rate of R . R is also positive. \bar{v} donates the average value of v , $B_v \geq 0$ donates the variation bound of v , and $B_{\dot{v}} \geq 0$ donates the maximum variation rate of v .

(III) Proposed Current Controller

A current controller can either control the current directly or control the current indirectly by controlling the flux linkage. For a certain position θ , ψ is a monotone increasing function of i . For any $i_1 \geq 0$, $i_2 \geq 0$ there is

$$\begin{aligned} \psi_m(\theta, i_1) &> \psi_m(\theta, i_2) \Leftrightarrow i_1 > i_2 \\ \psi_m(\theta, i_1) &= \psi_m(\theta, i_2) \Leftrightarrow i_1 = i_2 \\ \psi_m(\theta, i_1) &< \psi_m(\theta, i_2) \Leftrightarrow i_1 < i_2 \end{aligned} \quad (7)$$

Therefore, the phase current can be controlled by controlling its corresponding flux linkage. The SRM model shown in (4) contains unknown parameters, a current

controller with estimated parameter values could be constructed as

$$u_c = \hat{\alpha} \frac{d\psi_m(\theta, i_{ref})}{dt} + \hat{R}i_{ref} + \hat{v} + ke \quad (8)$$

where $\psi_m(\theta, i_{ref})$ is the reference flux linkage calculated by the reference current i_{ref} and rotor position θ , $\hat{\alpha}$ is the estimated value of α , \hat{R} is the estimated value of R , \hat{v} is the estimated value of v , k is a positive constant, and e is the flux linkage error which can be expressed as

$$e = \psi_m(\theta, i_{ref}) - \psi_m(\theta, i) \quad (9)$$

Substituting (8) into (5), the flux linkage error dynamics can be derived as

$$\begin{aligned} \dot{e} &= -\frac{k}{\alpha}e - \hat{R}e_i + \frac{1}{\alpha}\hat{\alpha}\psi_m(\theta, i_{ref}) + \frac{1}{\alpha}\hat{R}i + \frac{1}{\alpha}\hat{v} \\ \hat{\alpha} &= \alpha - \tilde{\alpha} \\ \hat{R} &= R - \tilde{R} \\ \hat{v} &= v - \tilde{v} \\ e_i &= i_{ref} - i \end{aligned} \quad (10)$$

where $\tilde{\alpha}$, \tilde{R} and \tilde{v} are the estimation errors, e_i is the current error.

If a Lyapunov candidate is selected as

$$V = \frac{1}{2}e^2 + \frac{1}{2\alpha k_\alpha}\tilde{\alpha}^2 + \frac{1}{2\alpha k_R}\tilde{R}^2 + \frac{1}{2\alpha k_v}\tilde{v}^2 \quad (11)$$

where k_α , k_R , and k_v are positive constants. Then, the derivative of the Lyapunov candidate is

$$\begin{aligned} \dot{V} &= -\frac{k}{\alpha}e^2 - \frac{\hat{R}}{\alpha}ee_i \\ &\quad + \frac{1}{\alpha}\hat{\alpha}\psi_m(\theta, i_{ref})e - \frac{1}{\alpha k_\alpha}\tilde{\alpha}\dot{\tilde{\alpha}} \\ &\quad + \frac{1}{\alpha}\hat{R}ie - \frac{1}{\alpha k_R}\tilde{R}\dot{\tilde{R}} \\ &\quad + \frac{1}{\alpha}\hat{v}e - \frac{1}{\alpha k_v}\tilde{v}\dot{\tilde{v}} \\ &\quad + \frac{\tilde{\alpha}\dot{\tilde{\alpha}}}{\alpha k_\alpha} + \frac{\tilde{R}\dot{\tilde{R}}}{\alpha k_R} + \frac{\tilde{v}\dot{\tilde{v}}}{\alpha k_v} \end{aligned} \quad (12)$$

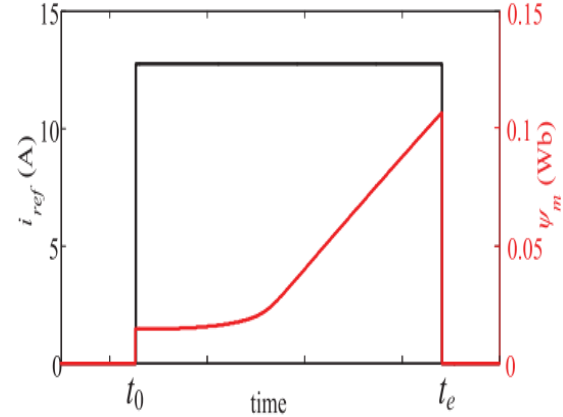


Fig. 2.2. Typical waveform of $\psi_m(\theta, i_{ref})$ and i_{ref}

It can be seen from (12) that if $\hat{\alpha}$, \hat{R} , and \hat{v} are chosen as

$$\begin{aligned} \hat{\alpha} &= k_\alpha \psi_m(\theta, i_{ref})e \\ \hat{R} &= k_R ie \\ \hat{v} &= k_v e \end{aligned} \quad (13)$$

Then, (12) becomes

$$\dot{V} = -\frac{k}{\alpha}e^2 - \frac{\hat{R}}{\alpha}ee_i + \frac{\tilde{\alpha}\dot{\tilde{\alpha}}}{\alpha k_\alpha} + \frac{\tilde{R}\dot{\tilde{R}}}{\alpha k_R} + \frac{\tilde{v}\dot{\tilde{v}}}{\alpha k_v} \quad (14)$$

(A) Constant Parameters

k , \hat{R} , and α are positive constants, and according to (7), e_i and e have the same sign. If α , R , v are constant, i.e.,

$$\dot{\tilde{\alpha}} = 0, \dot{\tilde{R}} = 0, \dot{\tilde{v}} = 0 \quad (15)$$

\dot{V} becomes

$$\dot{V} = -\frac{k}{\alpha}e^2 - \frac{\hat{R}}{\alpha}ee_i$$

Therefore \dot{V} is semi negative definite. This indicates that the system is globally asymptotically stable, and e is going to converge to zero. If e converges to zero, the system is internally stable. The convergence rate of e is determined by k and α . Since α is

around 1, k could be selected to adjust the convergence rate. According to (16), a larger k gives a faster convergence rate, which means faster dynamic response. However, according to (8), k is the feedback gain of the error, in this case, a large gain means that the controller is more sensitive to noise. Therefore, the selection of k is a tradeoff between the dynamic response and robustness. According to (10), if e converges to zero, for any $\psi_m(\theta, i_{ref})$ and i , there will be

$$\tilde{\alpha}\dot{\psi}_m(\theta, i_{ref}) + \tilde{R}i + \tilde{v} = 0 \quad (17)$$

As is known, the adaptive controllers suffer from parameter drafting. Since all the estimated parameters are bounded, the controller will be stable. However, parameters will not necessarily converge to their real values unless persistent excitation condition is satisfied [24]. For the case of (13), $\psi_m(\theta, i_{ref})$ and i need to be “rich” enough to guarantee the convergence. Fig. 3 shows a typical waveform of $\psi_m(\theta, i_{ref})$ and i_{ref} with flat-top current control. It can be seen that i_{ref} is a constant number and \dot{i}_{ref} is zero, while $\psi_m(\theta, i_{ref})$ is a nonlinear function of time.

The nonlinearity of $\psi_m(\theta, i_{ref})$ will provide sufficient frequencies to make $\psi_m(\theta, i_{ref})$ “rich.” This is another reason why flux linkage is selected to be controlled instead of current. In this case, there is

$$\Psi(t) = [\dot{\psi}_m(\theta, i_{ref}, t), 1]^T$$

$$\int_{t_0}^{t_e} \Psi(\tau) \Psi(\tau)^T d\tau \geq \gamma I \quad (18)$$

where t_0 is the beginning of each stroke and t_e is the end of the stroke. Equation (18) indicates that $\Psi(t)$ satisfies the exciting

condition, which means $\|\tilde{\alpha}\tilde{v}\|_2$ is going to converge per stroke [24]. In this case, as the controller is active each stroke, the estimation errors are going to converge to zero eventually and there will be

$$\begin{aligned} \hat{\alpha} &= \alpha \\ \hat{v} &= v \end{aligned} \quad (19)$$

However, if the flat-top current control is applied, i may not be rich enough to guarantee the convergence of \hat{R} . In this case, a dead zone should be added to prevent parameter drafting of \hat{R} .

(B) Variable Parameters

Practically, the parameters α , R , and v are not constant

$$\dot{\alpha} \neq 0, \dot{R} \neq 0, \dot{v} \neq 0 \quad (20)$$

Since α , R , and v have their own bounds, the adaption law in (13) should be modified by

$$\begin{aligned} \dot{\hat{\alpha}} &= \begin{cases} k_{\alpha} \dot{\psi}_m(\theta, i_{ref}) e, & \hat{\alpha} \in [\bar{\alpha} - B_{\alpha}, \bar{\alpha} + B_{\alpha}] \\ k_{\alpha} \dot{\psi}_m(\theta, i_{ref}) e, & \hat{\alpha} > \bar{\alpha} + B_{\alpha} \text{ and } \dot{\psi}_m(\theta, i_{ref}) e < 0 \\ k_{\alpha} \dot{\psi}_m(\theta, i_{ref}) e, & \hat{\alpha} < \bar{\alpha} - B_{\alpha} \text{ and } \dot{\psi}_m(\theta, i_{ref}) e > 0 \\ 0, & \text{else} \end{cases} \\ \dot{\hat{R}} &= \begin{cases} k_R i e, & \hat{R} \in [\bar{R} - B_R, \bar{R} + B_R] \\ k_R i e, & \hat{R} > \bar{R} + B_R \text{ and } i e < 0 \\ k_R i e, & \hat{R} < \bar{R} - B_R \text{ and } i e > 0 \\ 0, & \text{else} \end{cases} \\ \dot{\hat{v}} &= \begin{cases} k_v e, & \hat{v} \in [\bar{v} - B_v, \bar{v} + B_v] \\ k_v e, & \hat{v} > \bar{v} + B_v \text{ and } e < 0 \\ k_v e, & \hat{v} < \bar{v} - B_v \text{ and } e > 0 \\ 0, & \text{else.} \end{cases} \end{aligned} \quad (21)$$

This modification does not affect the system stability if the real values of α , R , and v do not exceed their bounds. At the same time, (22) defines the bounds of parameter estimation error

$$|\tilde{\alpha}| \leq 2B_{\alpha}, |\tilde{R}| \leq 2B_R, |\tilde{v}| \leq 2B_v \quad (22)$$

Combined with (3) and (6), there are

$$\frac{\hat{\alpha}^2}{2\alpha k_\alpha} + \frac{\hat{R}^2}{2\alpha k_R} + \frac{\hat{v}^2}{2\alpha k_v} \leq \frac{2B_\alpha^2}{\alpha k_\alpha} + \frac{2B_R^2}{\alpha k_R} + \frac{2B_v^2}{\alpha k_v} = M \quad (23)$$

$$\frac{\hat{\alpha}\dot{\alpha}}{\alpha k_\alpha} + \frac{\hat{R}\dot{R}}{\alpha k_R} + \frac{\hat{v}\dot{v}}{\alpha k_v} \leq \frac{2B_\alpha B_{\dot{\alpha}}}{\alpha k_\alpha} + \frac{2B_R B_{\dot{R}}}{\alpha k_R} + \frac{2B_v B_{\dot{v}}}{\alpha k_v} = N \quad (24)$$

where $B_{\dot{\alpha}}$, $B_{\dot{R}}$, and $B_{\dot{v}}$ are the bounds of $\dot{\alpha}$, \dot{R} , and \dot{v} , respectively. According to (14) and (11), there is

$$\begin{aligned} e^2 &= 2V - \frac{\hat{\alpha}^2}{\alpha k_\alpha} - \frac{\hat{R}^2}{\alpha k_R} - \frac{\hat{v}^2}{\alpha k_v} \\ \dot{V} &= -2\frac{k + k_i \hat{R}}{\alpha} \left(V - \frac{\hat{\alpha}^2}{2\alpha k_\alpha} - \frac{\hat{R}^2}{2\alpha k_R} - \frac{\hat{v}^2}{2\alpha k_v} \right) \\ &\quad + \frac{\hat{\alpha}\dot{\alpha}}{\alpha k_\alpha} + \frac{\hat{R}\dot{R}}{\alpha k_R} + \frac{\hat{v}\dot{v}}{\alpha k_v} \end{aligned} \quad (25)$$

Where $k_i > 0$ donates the relationship between e and \dot{e} . According to (25), if V exceeds $\alpha N/2(k + k_i \hat{R}) + M$, \dot{V} will be negative, and V is going to decrease. Thus, the control error is bounded by

$$\begin{aligned} |e| &\leq \sqrt{\alpha N/2(k + k_i \hat{R})} \\ &= \sqrt{\frac{2B_\alpha B_{\dot{\alpha}}}{(k + k_i \hat{R})k_\alpha} + \frac{2B_R B_{\dot{R}}}{(k + k_i \hat{R})k_R} + \frac{2B_v B_{\dot{v}}}{(k + k_i \hat{R})k_v}} \end{aligned} \quad (26)$$

As shown from (26), for the predefined bounds and maximum variation rates of the unknown parameter, the control error is limited by k , k_α , k_R , and k_v .

(C) Digital Implementation of Proposed Current Controller

In digital implementation, the discrete form of (8) and (21) can be reformulated as

$$\begin{aligned} \Delta\psi_m(k) &= \psi_m(\theta(k+1), i_{ref}(k+1)) - \psi_r \\ u_c(k) &= \hat{\alpha}(k) \frac{\Delta\psi_m(k)}{T} + \hat{R}(k) i_{ref}(k) + \end{aligned} \quad (27)$$

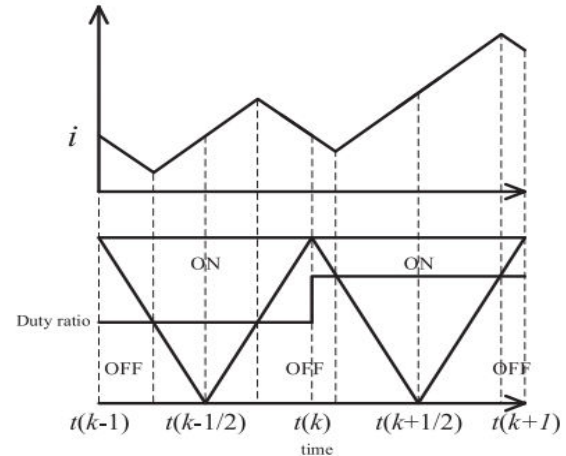


Fig. 3. PWM modulation

Where T is the digital sampling time, $\theta(k+1) = \theta(k) + \omega T$, and ω is the electric angular speed of the SRM

$$\begin{aligned} \hat{\alpha}(k+1)' &= \hat{\alpha}(k) + k_\alpha \Delta\psi_m(k) e(k) \\ \hat{\alpha}(k+1) &= \begin{cases} \hat{\alpha}(k+1)', & \hat{\alpha}(k+1)' \in [\bar{\alpha} - B_\alpha, \bar{\alpha} + B_\alpha] \\ \bar{\alpha} + B_\alpha, & \hat{\alpha}(k+1)' > \bar{\alpha} + B_\alpha \\ \bar{\alpha} - B_\alpha, & \hat{\alpha}(k+1)' < \bar{\alpha} - B_\alpha \end{cases} \\ e(k)' &= \begin{cases} e(k), & |e(k)| > BDZ \\ 0, & |e(k)| \leq BDZ \end{cases} \\ \hat{R}(k+1)' &= \hat{R}(k) + k_R i(k) e(k) T \\ \hat{R}(k+1) &= \begin{cases} \hat{R}(k+1)', & \hat{R}(k+1)' \in [\bar{R} - B_R, \bar{R} + B_R] \\ \bar{R} + B_R, & \hat{R}(k+1)' > \bar{R} + B_R \\ \bar{R} - B_R, & \hat{R}(k+1)' < \bar{R} - B_R \end{cases} \\ \hat{v}(k+1)' &= \hat{v}(k) + k_v e(k) T \\ \hat{v}(k+1) &= \begin{cases} \hat{v}(k+1)', & \hat{v}(k+1)' \in [\bar{v} - B_v, \bar{v} + B_v] \\ \bar{v} + B_v, & \hat{v}(k+1)' > \bar{v} + B_v \\ \bar{v} - B_v, & \hat{v}(k+1)' < \bar{v} - B_v \end{cases} \end{aligned} \quad (28)$$

Where $\Delta\psi_m(k)$ is defined in (27). BDZ is the error dead zone, $\bar{\alpha}$, \bar{R} , and \bar{v} are the estimated average values of α , R , and v , respectively.

(IV) PWM Delay Compensation

Fig. 3 shows the PWM modulation for digital control. The duty ratio is either obtained by u_c/UDC for soft chopping or $0.5 + 0.5(u_c/UDC)$ for hard chopping. UDC is the dc bus voltage. In the k th control period, current should be sampled at $t(k)$. But in practice, especially in a DSP control, if

current is sampled at $t(k)$, it will take some time for the controller to calculate the duty ratio and the duty ratio for $t(k)$ is actually loaded into the PWM modulator at $t(k+1)$. This brings one sampling time delay into the control loop. In this case, the duty ratio for $t(k)$ should be calculated before $t(k)$. Mohamed and El-Saadany [10] proposes a predictive current controller to solve

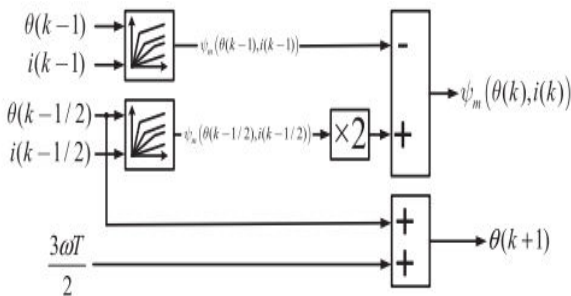


Fig. 4. Approximation of $i(k)$, $\theta(k)$, and $\theta(k+1)$

the problem. However, the predictive current controller needs accurate model and increases the calculation burden for DSP, especially for nonlinear systems such as SRMs. Blaabjerg et al.[9] recommends that current should be sampled at $t(k-1/2)$, which means $i(k)$ is approximated by

$$i(k) \approx i(k-1/2) \quad (29)$$

As shown in Fig. 3, there is no switching action at $t(k-1/2)$, EMI noise at that instance can be avoided. Furthermore, the duty ratio can be calculated within half of the period and delay in the control loop is avoided.

The estimation of (29) is accurate if the average current of each k th period stays the same, as the $(k-1)$ th period shown in Fig. 3. If average current between each period changes, as the k th period shown in Fig.4, (29) is not accurate.

As shown in Fig. 3, with the symmetrical modulation, the voltage waveforms of the former half period and the latter halfperiod are symmetric. Therefore, the flux could be estimated instead of current. The flux $\psi_m(\theta(k), i(k))$ could be approximated by

$$\begin{aligned} \psi_m(\theta(k), i(k)) &\approx 2\psi_m(\theta(k-1/2), i(k-1/2)) \\ &\quad - \psi_m(\theta(k-1), i(k-1)). \end{aligned} \quad (30)$$

In (30), current is sampled at both $t(k-1/2)$ and $t(k-1)$, which doubles the sampling rate. The ADCs used in motor control is capable of working at the sampling rate of twice of the PWM frequency without increasing any cost. Similar to (29), (30) also avoids the EMI noise caused by the switching action, provides half control period for duty ratio calculation, and avoids the delay in the control loop as well. Since the current sampling, and other calculations are performed at $t(k-1/2)$, the rotor position also has to be approximated with the information at $t(k-1/2)$. Fig. 4 shows the approximation of $\psi_m(\theta(k), i(k))$ and $\theta(k+1)$ for further use.

(A) Flux Reference Adjustment

When implemented in a digital processor, the current controller has to meet physical limits. Normally, when a phase is turned ON, the phase current is expected to rise quickly to the reference value, however, the voltage applied on the phase is limited by UDC. It is necessary to adjust $(\theta(k+1), i_{ref}(k+1))$

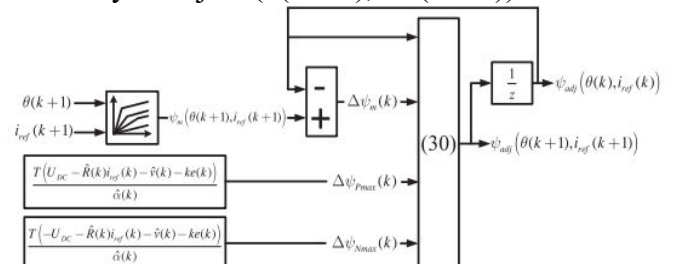


Fig. 5. Procedure of calculating $\psi_{adj}(\theta(k+1), i_{ref}(k+1))$ and $\psi_{adj}(\theta(k), i_{ref}(k))$.

so that $u_c(k)$ would not exceed UDC

$$\Delta\psi_m(k) = \psi_m(\theta(k+1), i_{ref}(k+1)) - \psi_{adj}(\theta(k), i_{ref}(k))$$

$$\Delta\psi_{Pmax}(k) = \frac{T(U_{DC} - \hat{R}(k)i_{ref}(k) - \hat{v}(k) - ke(k))}{\hat{\alpha}(k)}$$

$$\Delta\psi_{Nmax}(k) = \frac{T(-U_{DC} - \hat{R}(k)i_{ref}(k) - \hat{v}(k) - ke(k))}{\hat{\alpha}(k)}$$

$$\psi_{adj}(\theta(k+1), i_{ref}(k+1)) = \psi_{adj}(\theta(k), i_{ref}(k))$$

$$+ \begin{cases} \Delta\psi_{Pmax}(k), & \Delta\psi_m(k) > \Delta\psi_{Pmax}(k) \\ \Delta\psi_{Nmax}(k), & \Delta\psi_m(k) < \Delta\psi_{Nmax}(k) \\ \Delta\psi_m(k), & \Delta\psi_{Nmax}(k) \leq \Delta\psi_m(k) \leq \Delta\psi_{Pmax}(k). \end{cases}$$

(31)

Therefore, $\psi_m(\theta(k+1), i_{ref}(k+1))$ and $\psi_m(\theta(k), i_{ref}(k))$ in (27) should be replaced by $\psi_{adj}(\theta(k+1), i_{ref}(k+1))$ and $\psi_{adj}(\theta(k), i_{ref}(k))$, respectively. Fig. 5 shows the procedure of calculating $\psi_{adj}(\theta(k+1), i_{ref}(k+1))$ and $\psi_{adj}(\theta(k), i_{ref}(k))$ according to (31). Fig. 6 shows the procedure of calculating, $\hat{\alpha}(k)$, $\hat{R}(k)$, and $\hat{v}(k)$ according to (28). Fig. 7 shows the procedure of calculating $u_c(k)$ according to (27).

(B). Relationship With Previously Proposed Controllers

As shown in Fig. 7, the controller of (27) consists of two parts: the feedback part and the feed forward part. The feedback part is sensitive to noise, while the feed forward part is immune to noise. In order to enhance the robustness of the controller, the feed forward part should give out most part of u_c so that less control effort is needed by the feedback part.

The digital controller of (27) has similar form with previously proposed controllers. For example, all the estimated parameters are taken as its real value, and $k = 1/T$, then (27) becomes

$$u_c(k) = \frac{\psi_m(\theta(k+1), i_{ref}(k+1)) - \psi_m(\theta(k), i(k))}{T} + Ri(k) + v. \quad (32)$$

This is a typical dead-beat controller proposed in [18]–[21]. If $\hat{\alpha}$ is fixed as $K_p \cdot T$ and only the adaption of \hat{v} is active with a

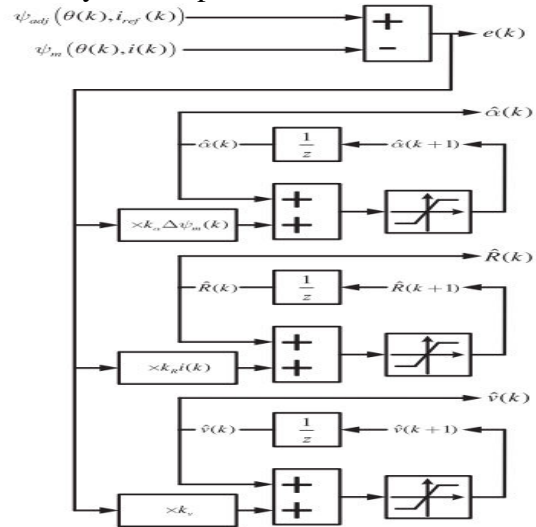


Fig.6. Procedure of calculating e , $\hat{\alpha}(k)$, $\hat{R}(k)$, and $\hat{v}(k)$

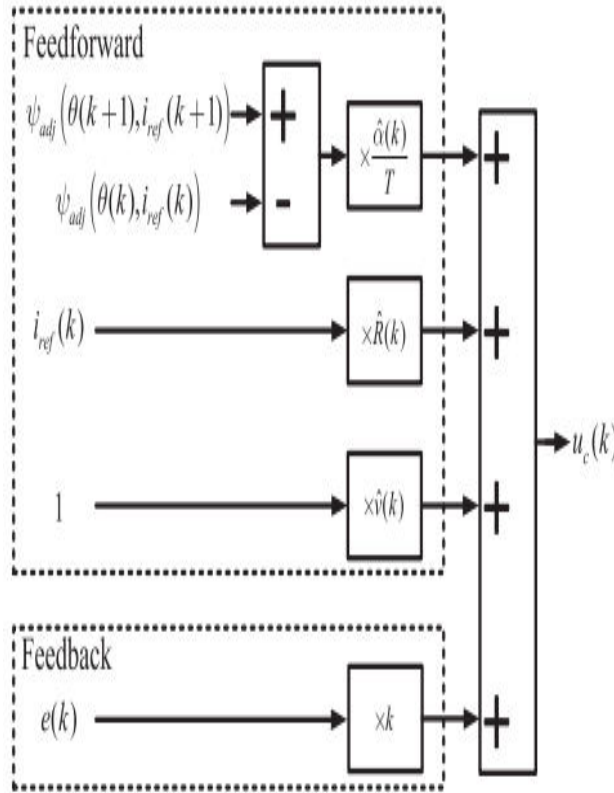


Fig. 7. Procedure of calculating $u_c(k)$ gain of K_i , then (27) becomes a PI controller

$$u_c(k) = K_p (\psi_m(\theta(k+1), i_{ref}(k+1)) - \psi_m(\theta(k), i(k))) + R i(k) + \hat{v}(k)$$

$$\hat{v}(k+1) = \hat{v}(k) + K_i e(k) T.$$
(33)

From this point of view, the proposed controller could be regarded as the improvement of some of the existing controllers.

(D) Parameter Selection

With the digital controller in (27), the error transfer function(10) could be rewritten in discrete domain as

$$e(k+2) = \left(1 - \frac{k}{\alpha} T\right) e(k+1) - \hat{R}(k+1) T e_i(k+1) + \frac{1}{\alpha} \hat{\alpha}(k+1) \Delta \psi_{adj}(\theta(k+1), i_{ref}(k+1)) + \frac{1}{\alpha} T \hat{R}(k+1) i(k+1) + \frac{1}{\alpha} T \hat{v}(k+1)$$
(34)

Since the sampling time T is usually small enough, substituting(28) into (34), the error dynamics can be obtained as

$$e z^2 - \left(1 - \frac{k}{\alpha} T\right) e z + P e = O$$

$$P = k_\alpha \frac{\Delta \psi_{adj}(\theta(k), i_{ref}(k)) \Delta \psi_{adj}(\theta(k+1), i_{ref}(k+1))}{\alpha} + k_R \frac{i(k+1) i(k)}{\alpha} T^2 + k_v \frac{1}{\alpha} T^2$$
(35)

where O is small enough bounded items, which could be taken as input of the error dynamic. The poles of the discrete transfer function of (35) are

$$\lambda_{1,2} = \frac{(1 - \frac{k}{\alpha} T) \pm \sqrt{(1 - \frac{k}{\alpha} T)^2 - 4P}}{2}$$
(36)

To stabilize the system, the poles should be placed inside the unit cycle, and hence the limits of the parameters are

$$0 < \frac{k}{\alpha} T < 2 + P$$

$$0 < P < \frac{1}{4}$$
(37)

It can be seen that in (32), k is selected to be $1/T$ and P is selected to be zero, and therefore, the poles are placed at zero. Due to the feed forward part in the proposed controller, a smaller k could be chosen. After k is chosen, k_α , k_R , and k_v are selected to ensure the stability.

(V) ANFIS CONTROLLER



(A) Adaptive Neuro-Fuzzy Inference Systems: (ANFIS):

An adaptive neuro-fuzzy inference system or adaptive network-based fuzzy inference system (ANFIS) is a kind of artificial neural network that is based on Takagi–Sugeno fuzzy inference system. The technique was developed in the early 1990s. Since it integrates both neural networks and fuzzy logic principles, it has potential to capture the benefits of both in a single framework. Its inference system corresponds to a set of fuzzy IF–THEN rules that have learning capability to approximate nonlinear functions. Hence, ANFIS is considered to be a universal estimator. For using the ANFIS in a more efficient and optimal way, one can use the best parameters obtained by genetic algorithm.

The adaptive network based fuzzy inference system (ANFIS) is a data driven procedure representing a neural network approach for the solution of function approximation problems. Data driven procedures for the synthesis of ANFIS networks are typically based on clustering a training set of numerical samples of the unknown function to be approximated. Since introduction, ANFIS networks have been successfully applied to classification tasks, rule-based process control, pattern recognition and similar problems. Here a fuzzy inference system comprises of the fuzzy model proposed by Takagi, Sugeno and Kang to formalize a systematic approach to generate fuzzy rules from an input output data set.

(B) ANFIS structure

For simplicity, it is assumed that the fuzzy inference system under consideration has two inputs and one output. The rule base

contains the fuzzy if-then rules of Takagi and Sugeno's type as follows:

If x is A and y is B then z is $f(x,y)$

where A and B are the fuzzy sets in the antecedents and $z = f(x, y)$ is a crisp function in the consequent. Usually $f(x, y)$ is a polynomial for the input variables x and y . But it can also be any other function that can approximately describe the output of the system within the fuzzy region as specified by the antecedent. When $f(x,y)$ is a constant, a zero order Sugeno fuzzy model is formed which may be considered to be a special case of Mamdani fuzzy inference system where each rule consequent is specified by a fuzzy singleton. If $f(x,y)$ is taken to be a first order polynomial a first order Sugeno fuzzy model is formed. For a first order two rule Sugeno fuzzy inference system, the two rules may be stated as:

Rule 1: If x is A_1 and y is B_1 then $f_1 = p_1x + q_1y + r_1$

Rule 2: If x is A_2 and y is B_2 then $f_2 = p_2x + q_2y + r_2$

Here type-3 fuzzy inference system proposed by Takagi and Sugeno is used. In this inference system the output of each rule is a linear combination of the input variables added by a constant term. The final output is the weighted average of each rule's output. The corresponding equivalent ANFIS structure is shown in Fig. 8.

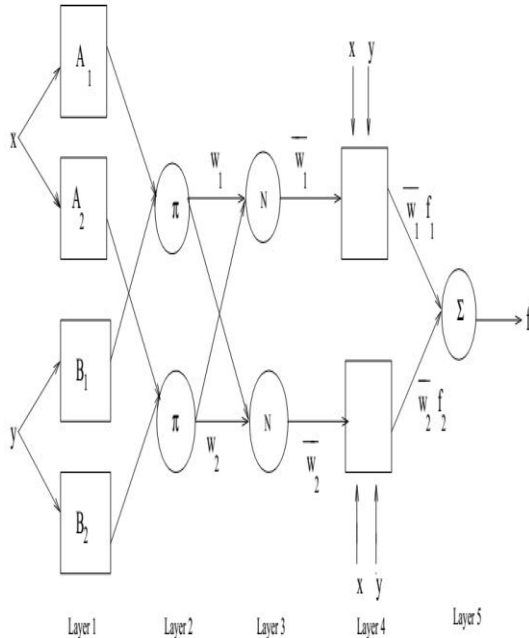


Figure 8: Type-3 ANFIS Structure

The individual layers of this ANFIS structure are described below:

Layer 1: Every node i in this layer is adaptive with a node function

$$O_i^1 = \mu_{A_i}(x) \quad (38)$$

where, x is the input to node i , A_i is the linguistic variable associated with this node function and μ_{A_i} is the membership function of A_i . Usually $\mu_{A_i}(x)$ is chosen as

$$\mu_{A_i}(x) = \frac{1}{1 + [(\frac{x-c_i}{a_i})^2]^{b_i}} \quad (39)$$

$$\mu_{A_i}(x) = \exp \left\{ -\left(\frac{x - c_i}{a_i} \right)^2 \right\} \quad (40)$$

where x is the input and $\{a_i, b_i, c_i\}$ is the premise parameter set.

Layer 2: Each node in this layer is a fixed node which calculates the firing strength w_i of a rule. The output of each node is the

product of all the incoming signals to it and is given by,

$$O_i^2 = w_i = \mu_{A_i}(x) \times \mu_{B_i}(y), \quad i = 1, 2 \quad (41)$$

Layer 3: Every node in this layer is a fixed node. Each i th node calculates the ratio of the i th rule's firing strength to the sum of firing strengths of all the rules. The output from the i th node is the normalized firing strength given by,

$$O_i^3 = \bar{w}_i = \frac{w_i}{w_1 + w_2}, \quad i = 1, 2 \quad (42)$$

Layer 4: Every node in this layer is an adaptive node with a node function given by

$$O_i^4 = \bar{w}_i f_i = \bar{w}_i (p_i x + q_i y + r_i), \quad i = 1, 2 \quad (43)$$

where \bar{w}_i is the output of Layer 3 and $\{p_i, q_i, r_i\}$ is the consequent parameter set.

Layer 5: This layer comprises of only one fixed node that calculates the overall output as the summation of all incoming signals, i.e.

$$O_i^5 = \text{overall output} = \sum_i \bar{w}_i f_i = \frac{\sum_i w_i f_i}{\sum_i w_i} \quad (44)$$

(D) Learning Algorithm

In the ANFIS structure, it is observed that given the values of premise parameters, the final output can be expressed as a linear combination of the consequent parameters.

The output f in Fig. 8 can be written as

$$\begin{aligned} f &= \frac{w_1}{w_1 + w_2} f_1 + \frac{w_2}{w_1 + w_2} f_2 \\ &= \bar{w}_1 f_1 + \bar{w}_2 f_2 \\ &= (\bar{w}_1 x) p_1 + (\bar{w}_1 y) q_1 + (\bar{w}_1) r_1 + (\bar{w}_2 x) p_2 + \end{aligned} \quad (45)$$

Where f is linear in the consequent parameters ($p_1, q_1, r_1, p_2, q_2, r_2$).

In the forward pass of the learning algorithm, consequent parameters are identified by the least squares estimate. In the backward pass, the error signals, which are the derivatives of the squared error with respect to each node output, propagate backward from the output layer to the input layer. In this backward pass, the premise parameters are updated by the gradient descent algorithm.

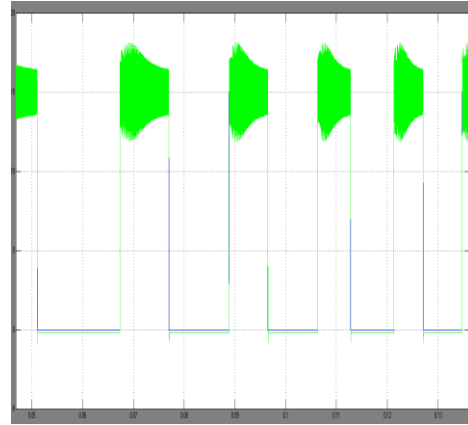


Fig. 10. Phase current and its reference with hysteresis current controller at 1000 r/min

(VI) SIMULATION RESULTS

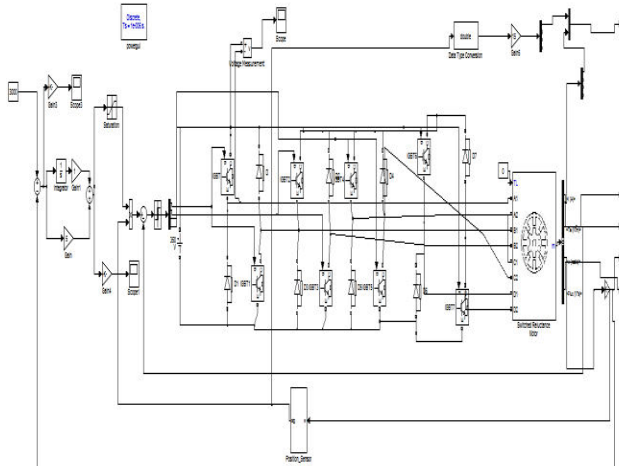


FIG9 SIMULINK DIAGRAM OF EXISTING SYSTEM

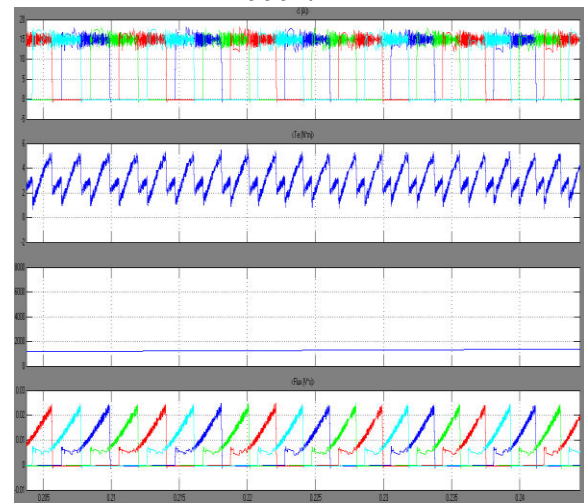


Fig. 11. Waveforms of control error(e), $\hat{\alpha}$, \hat{R} , and \hat{v} .

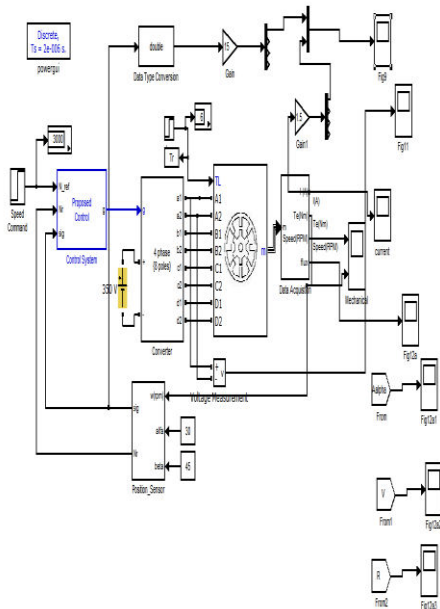


FIG12 SIMULINK DIAGRAM OF
PROPOSED SYSTEM

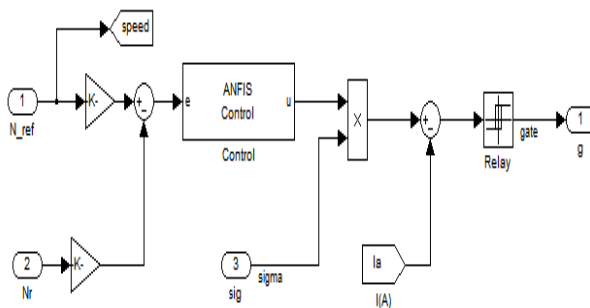


Fig13 SIMULINK DIAGRAM OF
PROPOSED SYSTEM CONTROLLER

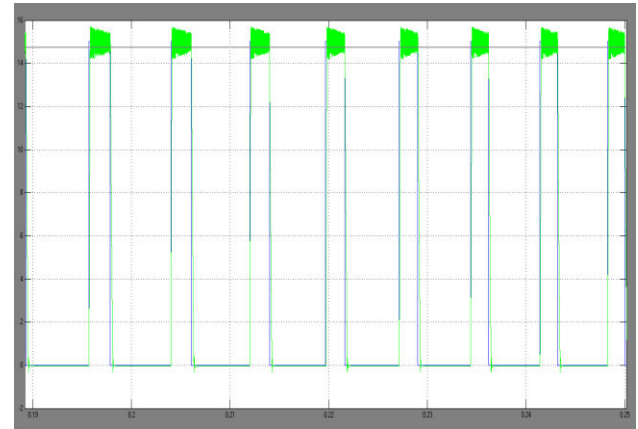


Fig. 14. Phase current and its reference with
proposed current controller at
1000 r/min.

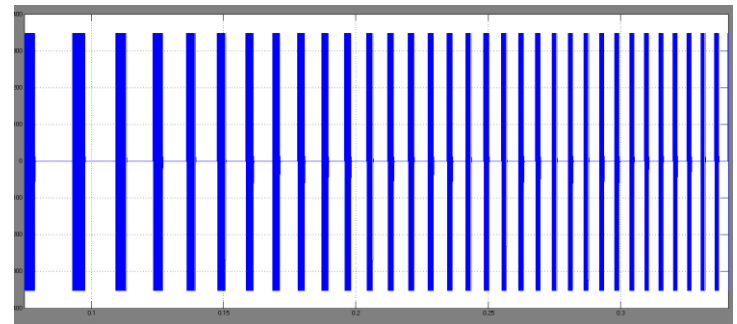


Fig. 15. Calculated uc of one phase during
the simulation at 1000 r/min.

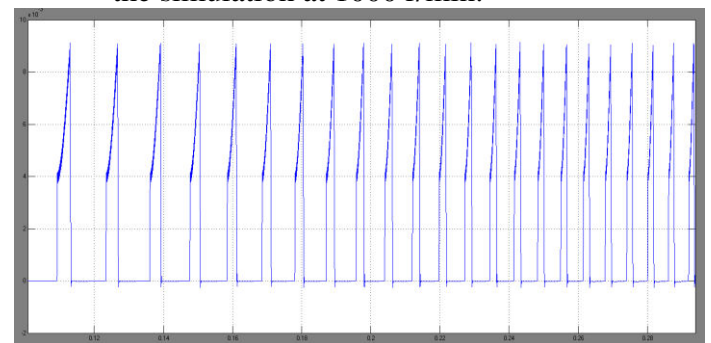
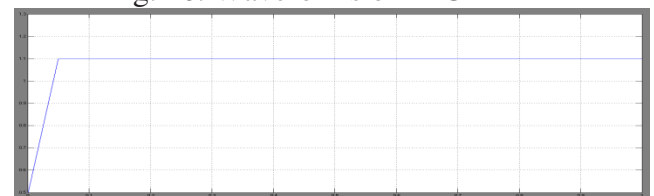


Fig. 16. Waveforms of FLUX



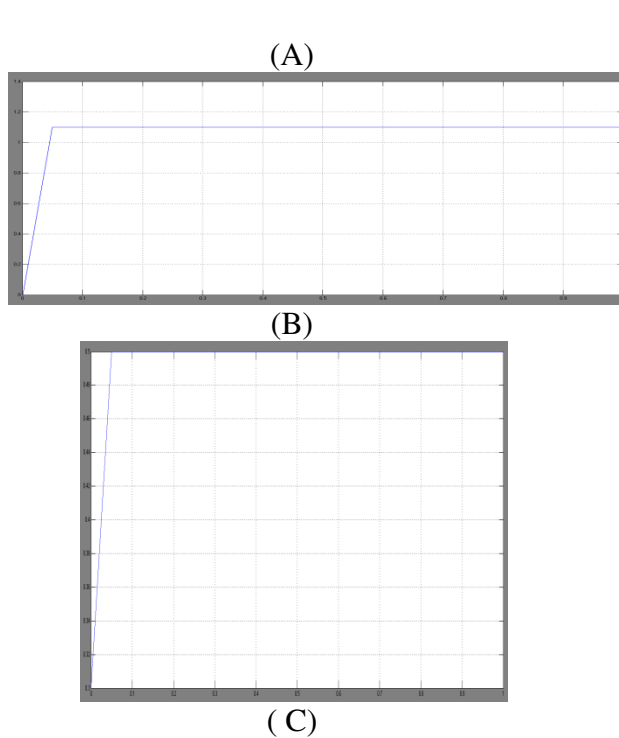


Fig. 17. Waveforms of control error(e), $\hat{\alpha}$, \hat{R} , and \hat{v} .

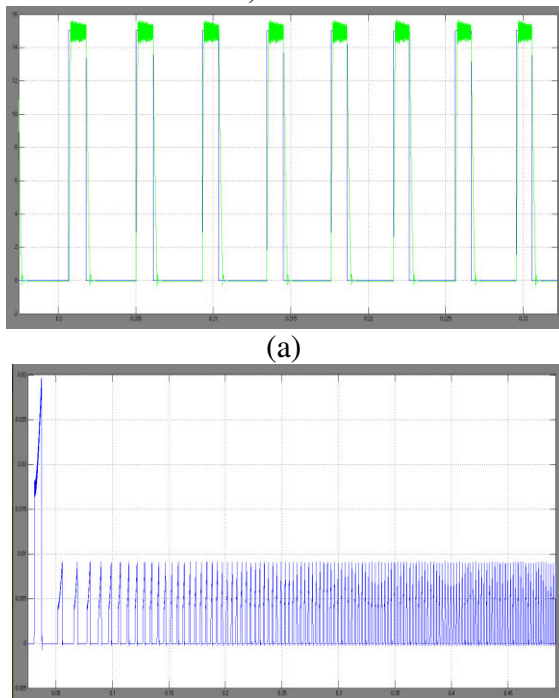


Fig. 18. Phase current, current reference, the original flux linkage reference $\psi_m(\theta, i_{ref})$, and the adjusted flux linkage reference $\psi_{adj}(\theta, i_{ref})$ at 6000 r/min.
(a) Phase current and its reference with proposed current controller at 6000 r/min.
(b) Original flux linkage reference $\psi_m(\theta, i_{ref})$, and the adjusted flux linkage reference $\psi_{adj}(\theta, i_{ref})$ at 6000 r/min.

VII. CONCLUSION

ANFIS based torque controller has been presented in this paper for tractive application at low speeds. By using ANFIS controller, the SRM exhibits good steady-state and dynamic performances. The SRM can produce maximum torque quickly while needing short duration overload ability.

REFERENCES

- [1] A. Emadi, Energy-Efficient Electric Motors: Selection and Applications. New York, NY, USA: Marcel Dekker, Sep. 2004.
- [2] J.-W. Ahn, S.-G. Oh, J.-W. Moon, and Y.-M. Hwang, "A three-phaseswitched reluctance motor with two-phase excitation," IEEE Trans. Ind. Appl., vol. 35, no. 5, pp. 1067–1075, Oct. 1999.
- [3] J.-W. Ahn, S.-J. Park, and D.-H. Lee, "Hybrid excitation of SRM for reduction of vibration and acoustic noise," IEEE Trans. Ind. Electron., vol. 51, no. 2, pp. 374–380, Apr. 2004.
- [4] D.-H. Lee, Z.-G. Lee, and J.-W. Ahn, "Instantaneous torque control of SRM with a logical torque sharing method," in Proc. IEEE Power Electron. Spec. Conf., Orlando, FL, USA, Jun. 2007, pp. 1784–1789.



- [5] H. Goto, A. Nishimiya, H.-J. Guo, and O. Ichinokura, "Instantaneous torque control using flux-based commutation and phase-torque distribution technique for SR motor EV," *COMPEL: Int. J. Comput. Math. Electr. Electron. Eng.*, vol. 29, no. 1, pp. 173–186, Jan. 2010.
- [6] J. Ye, B. Bilgin, and A. Emadi, "An extended-speed low-ripple torque control of switched reluctance motor drives," *IEEE Trans. Power Electron.*, vol. 30, no. 3, pp. 1457–1470, Mar. 2015.
- [7] J. Ye, B. Bilgin, and A. Emadi, "An offline torque sharing function for torque ripple reduction in switched reluctance motor drives," *IEEE Trans. Energy Convers.*, vol. 30, no. 2, pp. 726–735, Jun. 2015.
- [8] W. Cai and F. Yi, "An integrated multiport power converter with small capacitance requirement for switched reluctance motor drive," *IEEE Trans. Power Electron.*, vol. 31, no. 4, pp. 3016–3026, Apr. 2016.
- [9] F. Blaabjerg, P. Kjaer, P. Rasmussen, and C. Cossar, "Improved digital current control methods in switched reluctance motor drives," *IEEE Trans. Power Electron.*, vol. 14, no. 3, pp. 563–572, May 1999.
- [10] Y.-R. Mohamed and E. El-Saadany, "Robust high bandwidth discrete time predictive current control with predictive internal Model A unified approach for voltage-source PWM converters," *IEEE Trans. Power Electron.*, vol. 23, no. 1, pp. 126–136, Jan. 2008.
- [11] S. Schulz and K. Rahman, "High-performance digital PI current regulator for EV switched reluctance motor drives," *IEEE Trans. Ind. Appl.*, vol. 39, no. 4, pp. 1118–1126, Jul. 2003.
- [12] B. Shao and A. Emadi, "A digital PWM control for switched reluctance motor drives," presented at the *IEEE Vehicle Power Propulsion Conf.*, Lille, France, Sep. 2010.
- [13] R. Cardenas, R. Pena, M. Perez, J. Clare, G. Asher, and P. Wheeler, "Control of a switched reluctance generator for variable-speed wind energy applications," *IEEE Trans. Energy Convers.*, vol. 20, no. 4, pp. 781–791, Dec. 2005.
- [14] I. Husain and M. Ehsani, "Torque ripple minimization in switched reluctance motor drives by PWM current control," *IEEE Trans. Power Electron.*, vol. 11, no. 1, pp. 83–88, Jan. 1996.
- [15] H. Vasquez and J. K. Parker, "A new simplified mathematical model for a switched reluctance motor in a variable speed pumping application," *Mechatronics*, vol. 14, no. 9, pp. 1055–1068, Nov. 2004.